

## Research Article

# Investigating a Novel Hot Melt Extrusion-Based Drying Technique to Solidify an Amorphous Nanosuspension Using Design of Experiment Methodology

Bhavin Y. Gajera,<sup>1,3</sup> Dhaval A. Shah,<sup>2</sup> and Rutesh H. Dave<sup>3,4</sup>

Received 15 July 2018; accepted 17 September 2018; published online 2 October 2018

**Abstract.** The hot melt extrusion (HME) technology was explored and optimized to solidify an amorphous nanosuspension using Quality by Design (QbD) methodology. A design of experiments (DoE) approach was used to perform a set of 15 experiments, varying independent variables (feed rate, input temperature, and screw speed) within a design space. Redispersibility index (RDI), moisture content, and process yield constituted the critical quality attributes (CQAs) of the experimental design. Regression analysis and ANOVA were employed to identify and estimate significant main effects and two-way interactions, and model the process of HME drying for predictive purposes. The optimized HME-dried end product was characterized for physicochemical properties using differential scanning calorimetry (DSC), X-ray powder diffractions (XRPD), polarized light microscopy (PLM), Fourier transform infrared spectroscopy (FTIR), and *in vitro* dissolution studies. The statistical analysis reveals feed rate and input temperature as significant independent variables, critically influencing RDI and moisture content of solidified end product. The model developed for process yield was insignificant at a *p*-value of 0.05. The API retained its amorphous nature after the extrusion process which was confirmed using DSC and XRPD techniques. PLM was unsuitable to differentiate and determine crystallinity of drug moiety in the presence of a semi-crystalline bulking agent, microcrystalline cellulose (MCC). *In vitro* dissolution study depicted solubility and dissolution enhancement for HME-dried amorphous nanosuspension in both the dissolution media which can be attributed to amorphous nature of nanosized drug particles. A well-designed study implemented by DoE aided in developing a robust and novel HME technique to dry aqueous nanosuspension.

**KEY WORDS:** amorphous nanosuspension; design of experiment; hot melt extrusion; optimization; dissolution rate; analysis of variance (ANOVA).

## INTRODUCTION

Most of the current drugs, new chemical entities (NCEs) in the research pipeline belong to the brick-dust category of drugs, which faces solubility and dissolution rate limited bioavailability concerns (1,2). Presystemic metabolism and food effects further lead to increased inter-patient variability with regard to drug's absorption and systemic circulation. Higher doses have to be administered to achieve desired therapeutic plasma concentrations. Low solubility and dissolution rate have been counterbalanced by techniques such as complexation (3,4), salt formation (5), micronization (6),

nanonization (7), co-crystallization (8), and melt granulation (9,10). Techniques such as amorphization and nanonization of drugs are currently one of the most explored formulation strategies; wherein, amorphization leads to enhanced apparent saturation solubility of the drug by converting it to a high energy form and nanonization resulting in increased drug surface area promoting its dissolution rate (11,12).

Amorphous systems are disordered non-crystalline material, which has higher entropy, enthalpy, and free energy compared to other polymorphic forms of the drug. Since these amorphous systems are unstable, they are susceptible to crystallization prompting the formation of drug crystals which have relatively lower drug solubility (13–16). Amorphous systems can be stabilized by employing polymers which delay crystallization of system by either increasing the glass transition temperature (*T*<sub>g</sub>) of systems and/or drug-polymer interactions. The drug-polymer interactions lead to hydrogen bond formation and/or decrease in the free drug concentration available for nucleus formation. Additionally, high molecular weights and flexible polymeric conformation

<sup>1</sup> Impel NeuroPharma, Seattle, Washington, USA.

<sup>2</sup> Amneal Pharmaceuticals, Bridgewater Township, New Jersey, USA.

<sup>3</sup> Natoli Institute for Industrial Pharmacy Research and Development at Arnold and Marie Schwartz College of Pharmacy and Health Sciences, Long Island University, Brooklyn, New York 11201, USA.

<sup>4</sup> To whom correspondence should be addressed. (e-mail: rutesh.dave@liu.edu)

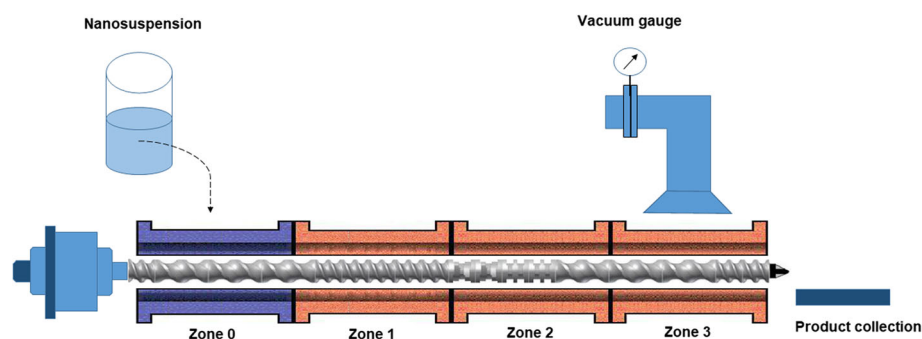


Fig. 1. HME assembly to dry clotrimazole nanosuspension

enable the polymers to prevent drug recrystallization, as it lowers the free energy of the amorphous systems (17,18). Nanoparticles are high-energy nanosized particles below 1  $\mu\text{m}$ , which augments dissolution rate and facilitates bioavailability. However, nanoparticles have higher Gibb's free energy which thermodynamically influences the particles to aggregate, thereby lowering associated Gibb's free energy. Nanoparticle aggregation can be delayed or avoided by incorporating high molecular weight polymers and surfactants which prevent particle aggregation by steric hindrance or electrostatic repulsion (19,20). "Nanoamorphous" technique involves reducing particle size to nano and amorphous form, which has synergistic benefits of the increased surface area and higher saturation solubility. There are currently only a few publications throwing light on the nanoamorphous formulation and its applications in pharmaceutical drug development (3,21–24).

A nanosuspension (crystalline or amorphous) is ultimately dried into solid powders for enhanced drug stability and commerciality. Matrix formers are inevitably added to the nanosuspensions before drying to produce stabilized dried nanoparticles. Sugars have been commonly used as matrix formers because of its property of embedding and/or adsorbing drug nanoparticles, and superior hydrophilicity, favoring rapid dissolution of drug particles. Mannitol, lactose, and trehalose are some of the commonly used matrix formers employed during drying of nanosuspensions (25–29). Insoluble excipients are occasionally used when sugars are insufficient in inhibiting particle agglomeration. MCC being water insoluble can form a permanent barrier between nanoparticles preventing agglomeration (30,31). An ideal matrix former should serve in two possible ways: (1) It should immobilize the nanoparticles by embedding it or layering it on matrix formers, and (2) it should not hinder the release of drug nanoparticles when contacted with an aqueous phase, resulting in rapid dissolution.

Table I. Independent Process Variables: Factors and Their Coded Levels

Factors	Low (-1)	Center (0)	High (+1)
Inlet temperature ( $^{\circ}\text{C}$ )	110	120	130
Feed rate (mL/min)	2.5	5	7.5
Screw speed (rpm)	100	150	200

There are various roadblocks to drying of nanosuspension by conventional drying techniques such as spray-drying, freeze-drying, pelletization, and granulation. These processes are time-consuming and difficult to scale up and are not cost-effective while developing or manufacturing a drug product. The conventional drying techniques are not well suited to be integrated into a continuous manufacturing environment. Hot melt extrusion has been an emerging technology which has viability for continuous manufacturing and is relatively easy to scale up (32). Baumgartner *et al.* have outlined several issues pertaining to conventional drying techniques while proposing a new NANEX technique to dry nanosuspension using hot melt extruder (33). The NANEX process involved introducing nanosuspension and matrix forming polymer through different zones, to embed drug nanoparticles into a polymeric matrix and simultaneously evaporating excess moisture content from the drug product. However, the introduction of nanosuspension and matrix forming polymer through different zones in an extruder can possibly lead to drug uniformity issues, especially in low-dose formulations.

The objective of the current study was to develop a QbD based novel nanosuspension drying technique using HME technology. Moreover, to overcome any possible uniformity issues and to simplify the drying process, MCC 101 was incorporated as a matrix former in the polymer stabilized nanosuspension. The nanosuspension was directly introduced in the extruder through a separate feeding device to evaporate the excess moisture and obtain dried nanosuspension. A vacuum assembly was installed at the rear end of the extruder to facilitate removal of excess moisture. Devolatilization of nanosuspension occurs by flash evaporation, and the use of appropriate vacuum pressure prevents any accumulation of moisture content in the end product. The nanoparticles during the course of being extruded get embedded into the polymer and matrix former producing a stable dried product. Furthermore, HME process parameters were optimized and validated, for solidifying nanosuspension by the design of experiments (DoE) methodology.

## MATERIALS AND METHODS

### Materials

The clotrimazole was purchased from Letco Medical (AL, USA). Soluplus<sup>®</sup> used as a polymeric stabilizer was purchased from BASF; microcrystalline cellulose 101 was purchased from FMC biopolymer (NJ, USA). HPLC grade

**Table II.** Box-Behnken Design Space for Drying of Clotrimazole Nanosuspension Using HME Process and Observed Responses

Run order	Input variables			Output variables		
	Inlet temperature (X1) °C	Screw speed (X2) (%)	Feed rate (X3) mL/min	Yield (Y1) % (w/w)	Moisture content (Y2) % (w/w)	RDI (Y3) (%)
1	110	100	5	84.73	5.15	108.97
2	130	100	5	85.16	4.34	163.76
3	110	200	5	81.33	5.57	131.94
4	130	200	5	85.82	4.83	182.76
5	110	150	2.5	82.9	4.88	103.73
6	130	150	2.5	87.09	3.86	140.31
7	110	150	7.5	84.28	6.04	131.11
8	130	150	7.5	86.39	5.47	217.88
9	120	100	2.5	83.44	4.46	109.33
10	120	200	2.5	82.12	4.98	113.91
11	120	100	7.5	88.24	5.29	163.41
12	120	200	7.5	80.04	5.86	190.00
13	120	150	5	82.61	4.22	121.43
14	120	150	5	83.17	4.29	121.74
15	120	150	5	84.68	4.41	123.91

ethanol, methanol, and TFA were purchased from Fisher Scientific (MA, USA). Hermetic pans and lids were purchased from TA instruments (DE, USA). Deionized (DI) water used was of reagent grade.

## Methods

### Formulation of Nanosuspension and Microsuspension

Clotrimazole drug was dissolved in ethanol to achieve a concentration of 60 mg/mL, forming a solvent (S) phase. Antisolvent (AS) phase comprised of Soluplus<sup>®</sup> dissolved separately in 100 mL of DI water at a concentration of 1.5% w/v. Antisolvent phase was maintained at 2°C during the entire process by a fluid mixture of propylene glycol and water *via* a recirculating chiller system. Solvent phase was injected into the AS phase using a syringe equipped with a needle gauge no. 22, while stirring at 2000 rpm. Sonication was performed during the process with the help of microtip sonicator for 30 s at 72 W. Sonication during the process assists in achieving a higher nucleation rate and prevents agglomeration of nanoparticles. The obtained nanosuspensions were stirred until used for HME drying process. MCC 101 was added as a bulking agent at a concentration of 7.9% w/v before drying. A microsuspension was prepared as a control, by physically mixing all the

ingredients mentioned above and continuously stirring it until used further for downstream processing.

### Drying of the Suspensions by HME

A twin-screw co-rotating hot melt extruder (OM10P, SteerAmerica, USA) was used to dry amorphous nanosuspension. The extruder has one non-heating zone and three heating zones which were optimally temperature regulated to dry nanosuspensions. As a part of preliminary screening study, three different screw sets (Do/Di: 1.27, 1.55, and 1.71) were utilized to evaluate the effect of different screw configurations on drying efficiency of nanosuspension. 1.71 Do/Di twin screws resulted in an end product with relatively lower moisture content. This was apparently due to a higher degree of fill and substantially higher residence time (56 s) compared to 1.27 and 1.55 screw sets. Thus, 1.71 twin screws were employed for all the future studies. A 1.71 Do/Di (Do-outer diameter; Di-inner diameter) screw configuration was used to perform extrusion runs. The clotrimazole nanosuspension at a rate of 2.5–7.5 mL/min was injected through zone 0 (Fig. 1). The zone 1 temperature was maintained at 130°C, whereas zone 2 and zone 3 were varied from 110 to 130°C as shown in Table I. Vacuum at a pressure of 150 mmHg was applied at zone 3 to remove any traces of moisture present in the sample thoroughly. Process parameters such as inlet temperature, screw speed, and feed rate were varied

**Table III.** Model Summary for Response Variables

Response variables	S	R-squared %	R-squared (adj) %	R-squared (pred) %
Process yield	1.3264	87.29	64.40	0.00
Moisture content	0.1914	86.78	81.00	78.01
RDI	4.7703	91.38	88.27	81.48

**Table IV.** ANOVA Response Table for Moisture Content of the HME-Dried Nanosuspension

Source	DF	Sum of squares	Mean square	F value	p value
Model	9	5.5191	0.61323	16.72	0.003
Temperature	1	1.1552	1.1552	31.5	0.002
Screw speed	1	0.23461	0.23461	6.4	0.053
Flow rate	1	2.43101	2.43101	66.3	0.000
Lack of fit	3	0.16488	0.05496	5.95	0.147

in accordance with the experimental design. The suspensions were continuously stirred during the entire process to maintain homogeneity. The resultant dried powders were accurately weighed and stored in silica gel desiccator until further studies.

### The Design of Experiments

The initial experimental studies helped in determining the suitable working range for all the process parameters. To optimize and evaluate the effect of process parameters on the product characteristics, a response surface design was generated using the Minitab<sup>®</sup> 17 software. Box-Behnken design (BBD) has been previously used to construct a three-factor, three-level design and has been efficient in exploring quadratic response surfaces and building a second-order polynomial model (34,35). Thus, a BBD consisting of 15 experiments with three center points was created using the Minitab<sup>®</sup> 17 software. Independent variables selected for the current study were inlet temperature (X1), feed rate (X2), and screw speed (X3). The levels of each variable are represented by a (+), (-), and (0) for higher, lower, and center levels respectively as shown in Table I. Product attributes measured for the current study were process yield (Y1), moisture content (Y2), and redispersibility index (RDI) (Y3). The Minitab<sup>®</sup> 17 software was used to calculate the expected form of the polynomial equation for each response variable:

$$Y = b_0 + b_1X_1 + b_2X_2 + b_3X_3 + b_{11}X_1^2 + b_{22}X_2^2 + b_{33}X_3^2 + b_{12}X_1X_2 + b_{13}X_1X_3 + b_{23}X_2X_3$$

where  $Y$  is the response variable,  $X$ 's are the input variables mentioned above, and the  $b$  parameters denote empirically derived coefficients characterizing the main ( $b_1, b_2, b_3$ ), interaction ( $b_{12}, b_{23}, b_{13}$ ), and the quadratic effects ( $b_{11}, b_{22}, b_{33}$ ) (36).

For validating the model generated by the software, optimal process parameters determined by response surface design were used to experimentally find the product characteristics and compare it with the predicted values. The relative error was calculated using the following equation (37):

$$\text{Relative error (\%)} = \frac{(\text{Predicted value} - \text{Experimental value})}{\text{Predicted value}} \times 100$$

### Statistical Analysis

**Regression and Modeling.** A polynomial equation was generated for all the response variables using the Minitab software. Regression analysis and analysis of variance (ANOVA) are some of the statistical tools which will be employed to understand the correlation between process parameters and response variables effectively.

**Response Surface Plots.** Response surface plots graphically explore the relationships between input parameters and one or more output parameters (38,39). The collected data sets facilitated in generating contour plots using the Minitab 17<sup>®</sup> software. The contour plots show the three-dimensional relationship in two dimensions, where input variables are plotted in  $x$ - and  $y$ -axis, and contours represent response variable.

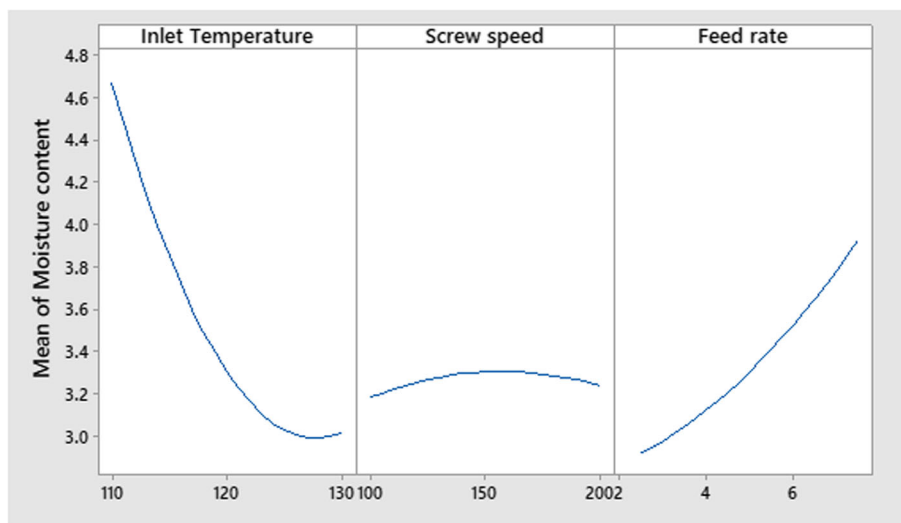


**Fig. 2.** Main effect plot for moisture content (% w/w), HME process

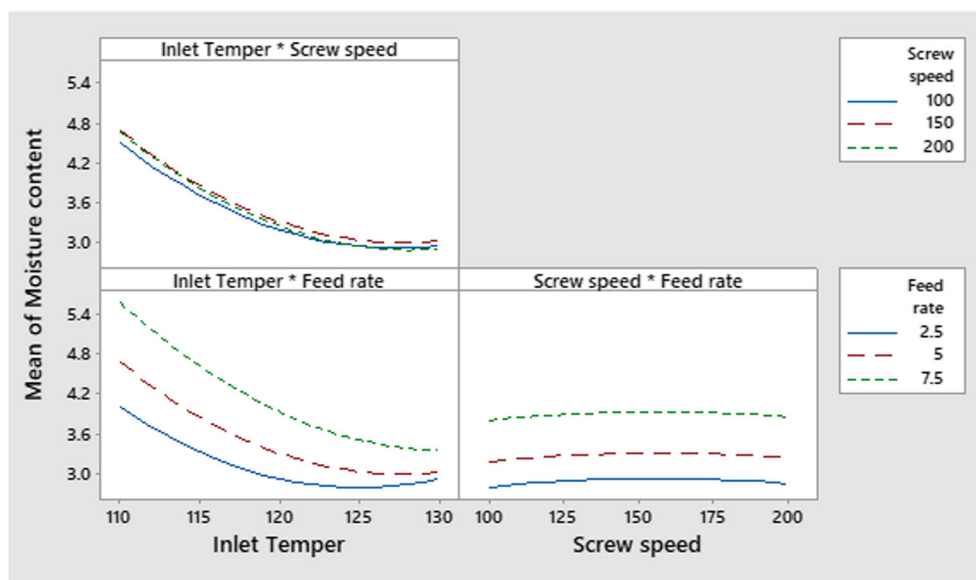


Fig. 3. Interaction effect plot for moisture content (% w/w), HME process

#### Polarized Light Microscopy Studies

For polarized light microscopy (PLM) studies, the analysis was performed using Axio Scope.A1 microscope (Zeiss, USA) with the help of the Captavision software. The solidified samples of nanosuspensions were dispersed in the mineral oil and placed on a clean glass slide. All the images were obtained at 10 $\times$  resolution under the dark field.

#### Differential Scanning Calorimetry Studies

Approximately  $5 \pm 1$  mg of samples were analyzed in a sealed aluminum pan with a pinhole under constant nitrogen purge, at a heating rate of 5°C/min from 20 to 400°C and modulated for  $\pm 0.796$ °C every 60 s (40). The Universal Analysis software (TA Instruments, USA) was used to

determine the heat of fusion and melting point for all the samples.

#### X-ray Powder Diffraction

X-ray powder diffraction measurements assessed the polymorphic structure of untreated and subsequently dried clotrimazole nanosuspension formulations at room temperature. XRPD analysis was performed on a Smart X-ray diffractometer (Rigaku, Japan) controlled by Smartlab Studio which includes Smartlab Guidance as the management system software and PDXL2 as the analysis software. X-ray radiation used was generated by copper K $\alpha$  filter method at 40 KV and 44 mA. Bragg-Brentano focusing geometry was used with ACS6 auto-sampler. A 0.2-mm deep, low background sample holder was used, and samples were scanned from 5 to 40 $^\circ$  two

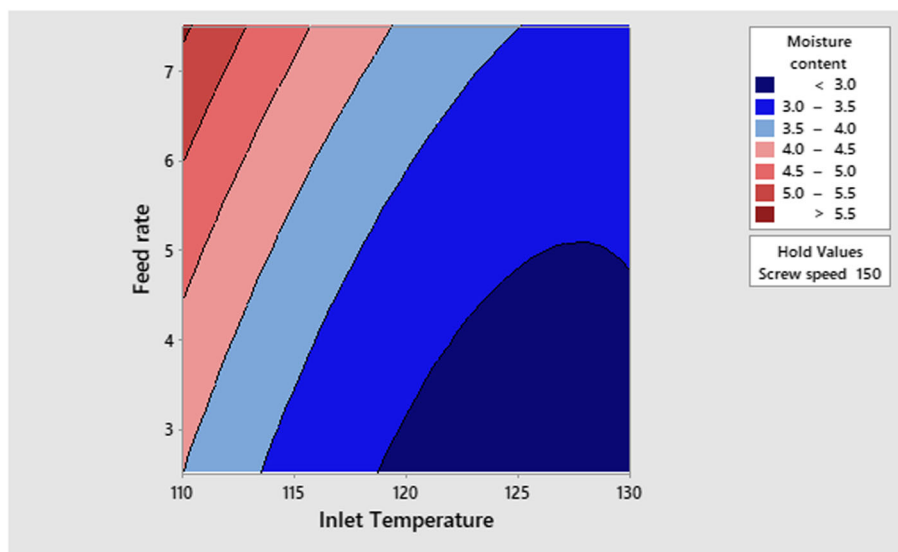


Fig. 4. Contour plot of moisture content (%w/w) vs. feed rate, inlet temperature

**Table V.** ANOVA Response Table for RDI of the HME-Dried Nanosuspension

Source	DF	Sum of squares	Mean of square	F value	p value
Model	9	18,349.7	2038.85	89.6	0.004
Inlet temperature	1	4180.9	4180.94	183.73	0.000
Screw speed	1	6.4	6.35	0.28	0.62
Feed rate	1	8268	8267.99	363.33	0.001
Lack of fit	3	95.7	31.91	3.54	0.228
Total	14	18,463.4			

theta at a scan rate of 3° per minute and scan step of 0.02°. Diffractograms were analyzed using the PDXL2 software.

#### Fourier Transform Infrared

Attenuated total reflectance (ATR) FTIR spectra were recorded using a Nicolet iS5 FTIR spectrophotometer with iD5 ATR diamond accessory (Thermo Fisher Scientific, USA). Samples were scanned between 4000 and 400 cm<sup>-1</sup> with an average of 64 scans and at a resolution of 4 cm<sup>-1</sup> by placing them on the diamond crystal and pressing the knob on it (41).

#### In Vitro Dissolution Studies

Dissolution study for the aqueous nanosuspension, HME-dried nanosuspension, and the physical mixture was conducted to determine and investigate the initial dissolution rate enhancement. Dissolution was carried out in USP Type-II (Paddle) dissolution apparatus at 75 rpm, maintained at 37 ± 0.5°C for 2 h. The dissolution medium for sink-condition dissolution consisted of 900 mL DI water and pH 7.2 buffer media. A 5 mL of a dissolution sample was withdrawn at 0, 2.5, 5, 7, 10, 15, 30, 45, 60, 90, and 120-min time points and replaced with the same volume of dissolution media (pre-equilibrated at 37 ± 0.5°). Samples were filtered through a 0.1-µm Anotop syringe filter before the HPLC analysis.

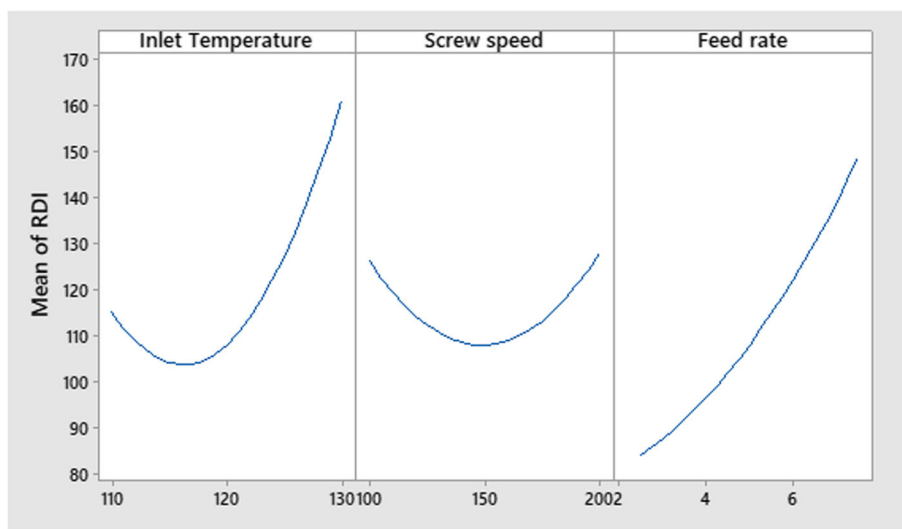
#### Loss on Drying

All the samples were subjected to loss on drying analysis to determine moisture retained in the end product after HME drying. The analysis was performed using an MB25 moisture analyzer equipped with a halogen lamp. The samples were dried at 105°C until a constant %LOD was obtained. Moisture content was calculated based on the weight change due to moisture loss and was expressed as a percentage by weight (%) (42). All the test was performed in triplicate.

#### Redispersibility Index Measurement

Redispersion studies of the solidified nanosuspension were performed in deionized water to investigate the effect of different processing conditions on aggregation tendency of nanoparticles after HME drying. Solidified nanosuspension is said to be completely redispersed when RDI value is close to 100%, indicating that the HME-dried nanoparticles are of the same size as those in the nanosuspension. HME-dried sample equivalent to 5 mg of clotrimazole was dispersed in 25 mL of deionized water and stirred at 200 rpm for 2 min before measuring the particle size. Redispersibility index (RDI) was calculated using the formula:

$$\text{RDI} = (D/D_0) \times 100\%$$

**Fig. 5.** Main effect plot for RDI (%), HME drying process



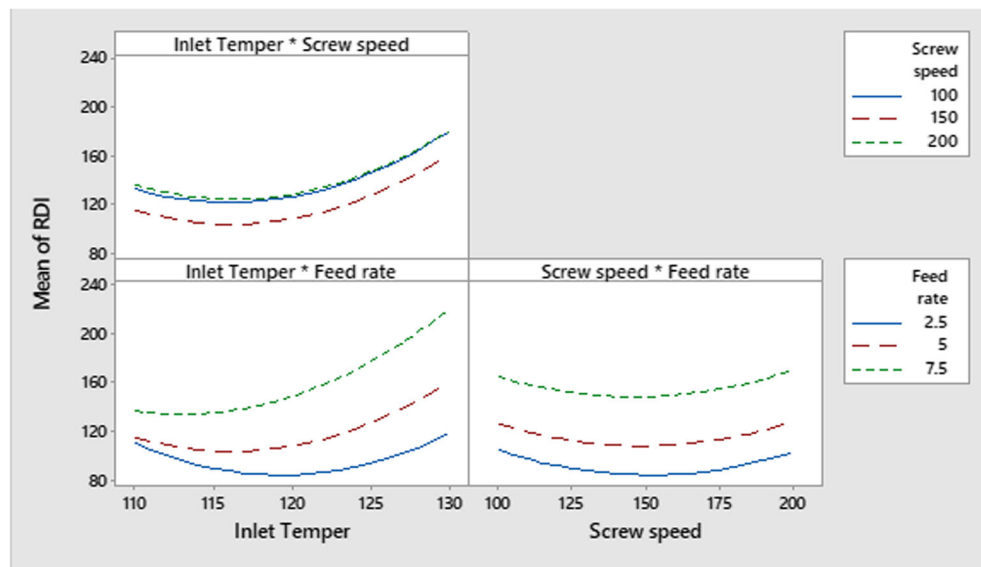


Fig. 6. Interaction effect plot for RDI (%), HME drying process

where  $D$  indicates the mean particle size of the redispersed suspension and  $D_0$  indicates the average particle size of the suspension before HME drying.

## RESULTS AND DISCUSSION

### DoE Analysis

The data was statistically analyzed using Minitab® to deconvolute the main and two-way interactions between process and formulation parameters. The three replicated center points in the experimental design helped in assessing the pure error of the experiment. Regression coefficients for each term are summarized and listed along with  $R^2$  of the regression model in Table II. The process yield ranged from 80.04 to 88.24% ( $w/w$ ), moisture content varied from 3.86 to 6.04%, and RDI ranged from 103.73 to 217.88% respectively.

### Effect of Process Parameters on Process Yield

From the ANOVA response table (not shown here), we can comment that the model could not appropriately fit the process yield data for dried clotrimazole nanosuspension at a 95% confidence interval and appears to be statistically insignificant ( $p$ -value  $> 0.05$ ). Furthermore, as seen in Table III, along with the low R-squared (adjusted) value, an R-squared (predicted) value of 0.00% shows the fallacy of the model in predicting the yield of the HME drying process. The process yield of HME process does not appear to follow a particular trend and could not be modeled for exploring main and interaction effects of formulation and process variables. HME process follows the principle of first in/first out since the material does not rotate along with the screw (43). Thus, unlike the spray-drying process, HME process parameters do not impact the overall yield of the drying process which is apparently advantageous for the overall productivity.

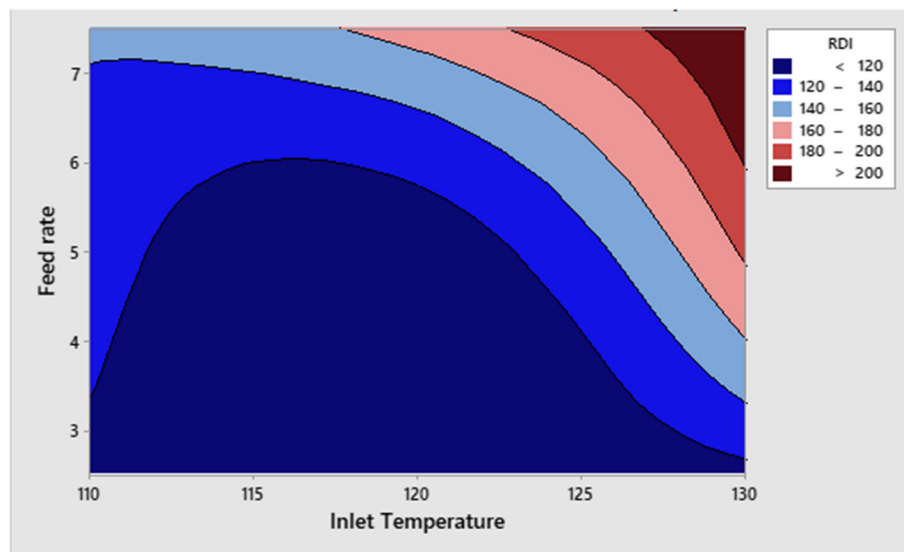


Fig. 7. Contour plot of RDI (%) vs. feed rate, inlet temperature

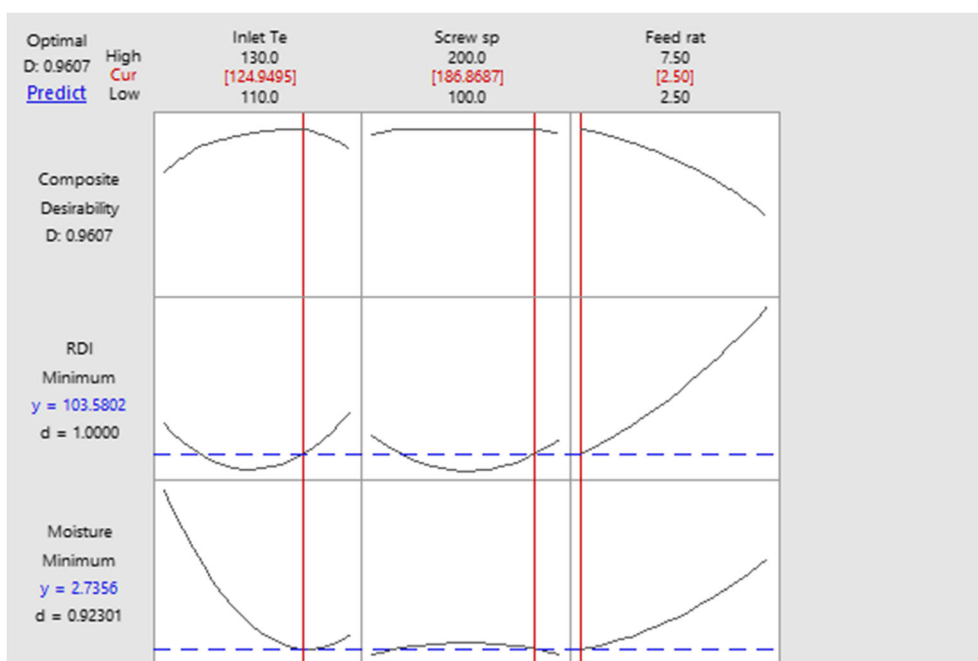


Fig. 8. Optimization plot for drying clotrimazole nanosuspension by HME

Effect of Process Parameters on the Moisture Content

The final polynomial model calculated for the response variable “moisture content” is as follows:

$$\begin{aligned} \text{Moisture content} = & 57.1 - 0.746 \text{ Temperature} - 0.0505 \text{ Screw speed} \\ & + 1.106 \text{ Flow rate} + 0.002867 \text{ Temperature} * \text{Temperature} \\ & + 0.000182 \text{ Screw speed} * \text{Screw speed} + 0.0751 \text{ Flow rate} * \text{Flow rate} \\ & - 0.000015 \text{ Temperature} * \text{Screw speed} + 0.00450 \text{ Temperature} \\ & * \text{Flow rate} + 0.000240 \text{ Screw speed} * \text{Flow rate} \end{aligned}$$

From the ANOVA response table (Table IV), we can comment that the model efficiently fits the moisture content data values for dried clotrimazole nanosuspension at a confidence interval of 95% with a *p*-value of 0.003. Furthermore, the model summary results (Table III) depict high R-squared and R-squared (adjusted) values. The R-squared (predicted) value of 78.01% shows suitable predictability of the model in predicting the moisture content of the HME-dried end products. As per the quadratic polynomial equation, inlet temperature negatively influences the moisture content of the final product; the flow rate is directly proportional to moisture content and leads to an increase in moisture content with an increase in flow rate. An increase in inlet temperature increases the overall thermal energy needed to evaporate the water content. An increase in feed

rate reduces the effectiveness of HME drying process, resulting in an HME-dried product with high moisture content. Thus, higher inlet temperature and lower flow rate led to the rapid and efficient removal of moisture from the nanosuspension. The quadratic and interaction effects of all the independent variables also significantly affected the final moisture content in the HME-dried product, which is further illustrated below using main plot, interaction effect plot, and contour plots. Conversely, screw speed does not have any significant effect on the moisture content of solidified nanosuspension.

Main and interaction effect plots as shown in Figs. 2 and 3 support the hypothesis proposed for inlet temperature, screw speed, and feed rate, based on the quadratic model equation for moisture content. Additionally, contour plots corroborate with the main effect plots and provide vital information about the design space which will lead to the lower moisture content in the HME-dried end product. From Fig. 4, we can state that low moisture content (% w/w) in the HME-dried product can be achieved at high temperature and low feed rate settings.

Effect of Process Parameters on the RDI

In the model for RDI, inlet temperature and feed rate have a negative main effect. Apart from these main effects, the quadratic effect of all the independent variables and interaction effect of inlet temperature-feed rate were the

Table VI. Multiple Response Prediction Tables for Drying of Clotrimazole Nanosuspension by HME

Response	Predicted	Observed	Relative error (%)
RDI (%)	103.58	108.12	4.38
Moisture content (% w/w)	2.73	2.57	5.86



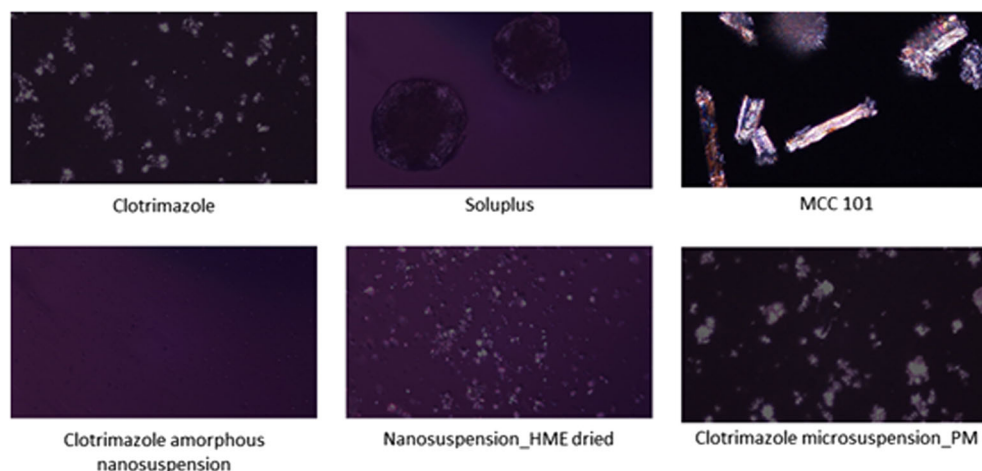


**Fig. 9.** PLM images of clotrimazole, Soluplus, MCC 101, amorphous nanosuspension, HME-dried nanosuspension, and PM microsuspension

most significant factors ( $p$ -value < 0.05) affecting the redispersibility of the HME-dried nanosuspension based on the statistical analysis.

The normal probability plot of the residuals (not shown here) shows some data points which do not fall precisely along a straight line passing through the center of the plot. However, the deviation from normality does not appear severe looking at lack of fit depicted in Table V. The final polynomial model calculated for determining the response variable, RDI, is as follows:

$$\begin{aligned} \text{RDI} = & 4738 - 73.45 \text{ Inlet Temperature} - 2.154 \text{ Screw speed} - 93.0 \text{ Feed rate} \\ & + 0.3008 \text{ Inlet Temperature} \times \text{Inlet Temperature} \\ & + 0.007601 \text{ Screw speed} \times \text{Screw speed} + 1.342 \text{ Feed rate} \\ & \times \text{Feed rate} - 0.00148 \text{ Inlet Temperature} \times \text{Screw speed} \\ & + 0.7525 \text{ Inlet Temperature} \times \text{Feed rate} + 0.0140 \text{ Screw speed} \\ & \times \text{Feed rate} \end{aligned}$$

As per the quadratic polynomial equation, inlet temperature negatively influences the RDI of the HME-dried product. The RDI of the HME-dried nanosuspension decreases with an increase in temperature until it reaches minima; thereafter, any increase in temperature leads to an increase in RDI (Fig. 5). At low-temperature settings, removal of moisture content is not efficient due to slower evaporation rate which leads to agglomeration of drug particles by formation of liquid bridges followed by its solidification, impacting the RDI of dried nanosuspension (44). At high-temperature conditions, residual moisture in the drug product is reduced efficiently. However, high-temperature settings along with high residence time promote aggregation of clotrimazole drug particles. Thus, moderate-temperature settings led to the efficient removal of residual moisture and resulted in lower RDI values compared to low- and high-temperature settings. The RDI appears to be directly proportional to the feed rate of clotrimazole nanosuspension in the HME extruder. At higher feed rate,

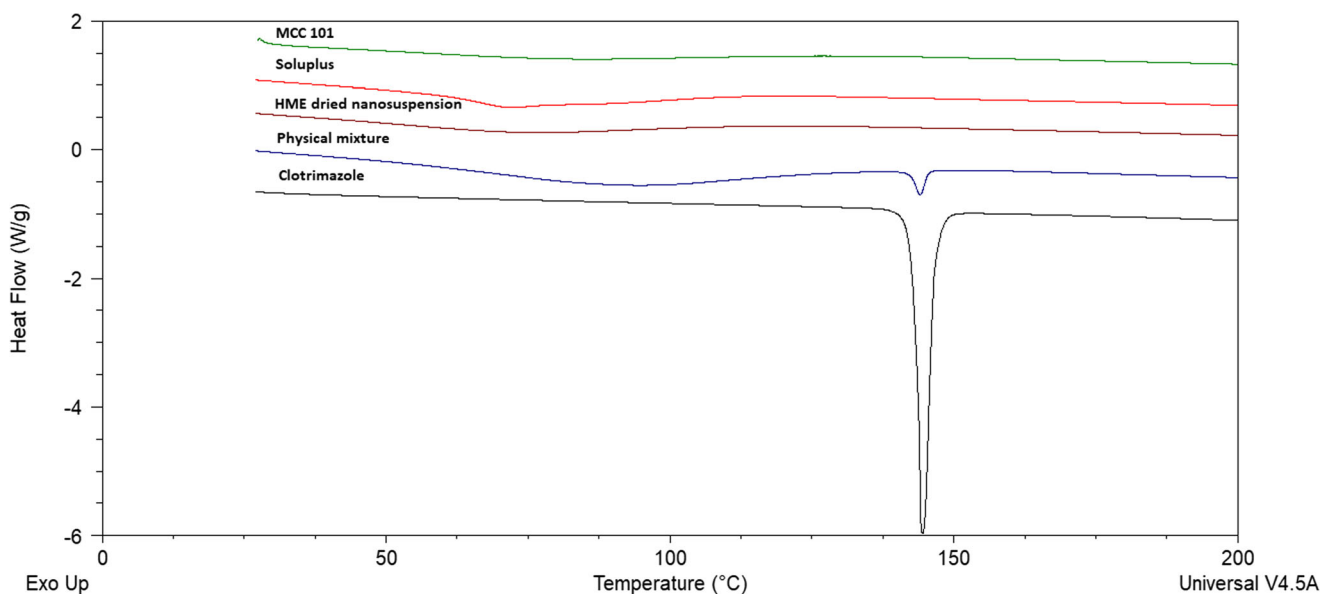


**Fig. 10.** DSC thermograms of crystalline clotrimazole, MCC 101, Soluplus, HME-dried nanosuspension, and PM microsuspension

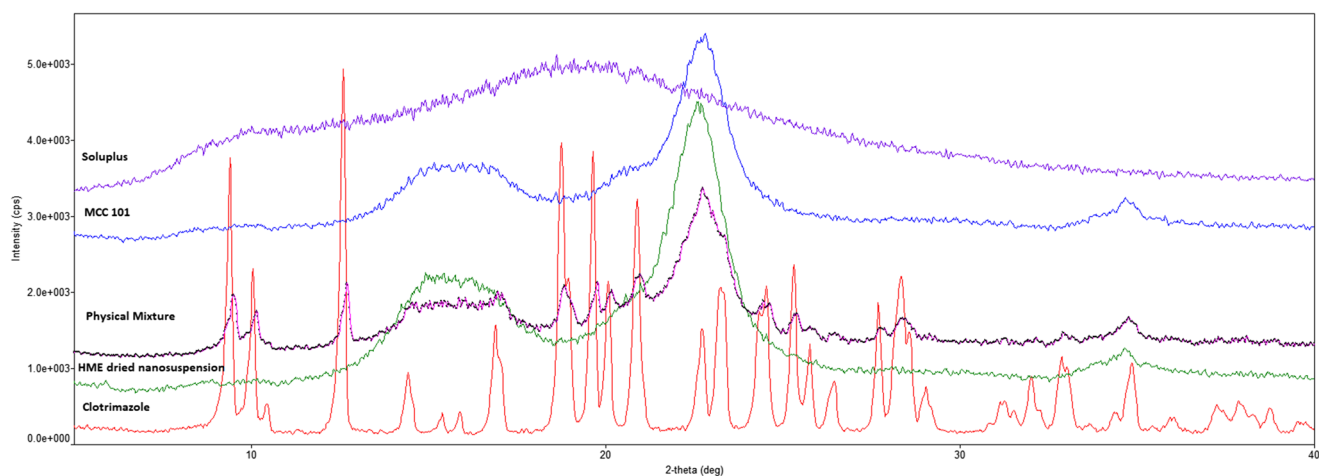


**Fig. 11.** XRPD thermograms of crystalline clotrimazole, MCC 101, Soluplus, HME-dried nanosuspension, and PM microsuspension

evaporation, and removal of moisture content were not efficiently achieved resulting in moisture-induced agglomeration of particles and subsequent higher RDI values. The screw speed of the extruder does not have any notable effect on the RDI of dried nanosuspension. The quadratic effect of inlet temperature and interaction effect of inlet temperature and feed rate significantly influence the RDI of HME-dried nanoparticles (Fig. 6).

Additionally, contour plots corroborate with the main effect and interaction effect plots and aid in elucidating the relationship between RDI and independent variables. As can be seen from Fig. 7, lower RDI numbers are achieved at moderate-temperature and lower feed rate settings.

#### Optimization and Validation

The most important aspect of performing DOE studies was to determine an optimum range of process parameters to achieve an HME-dried end product with low RDI, low moisture content, and high process yield. Therefore, after generating the polynomial equation correlating the response

and input variables, the process was optimized for the responses. Response surface methodology helps in solving the classic problem of process response maximum or minimum. This technique consists of searching for response surface maximum or minimum by carrying out experiments along a straight path whose direction is given by gradient analysis at specified points. The objective was to develop an efficient HME drying technique for clotrimazole nanosuspension which results in an RDI range of 100–110%. Low RDI values will ensure that colloidal amorphous nanoparticles still regain its original particle size after HME drying. The numerical optimization approach explores the design space, using the polynomial model developed during the analysis, to find the independent process parameter settings that meet the defined goals. The independent variable settings (inlet temperature—125°C, screw speed—187 rpm, and feed rate—2.5 mL/min) used for validation experiments were identified by optimization plot (Fig. 8). The predicted and experimentally determined response variables are listed in Table VI. The process yield was not taken into account during optimization since it was not critically affected by HME process parameters. The

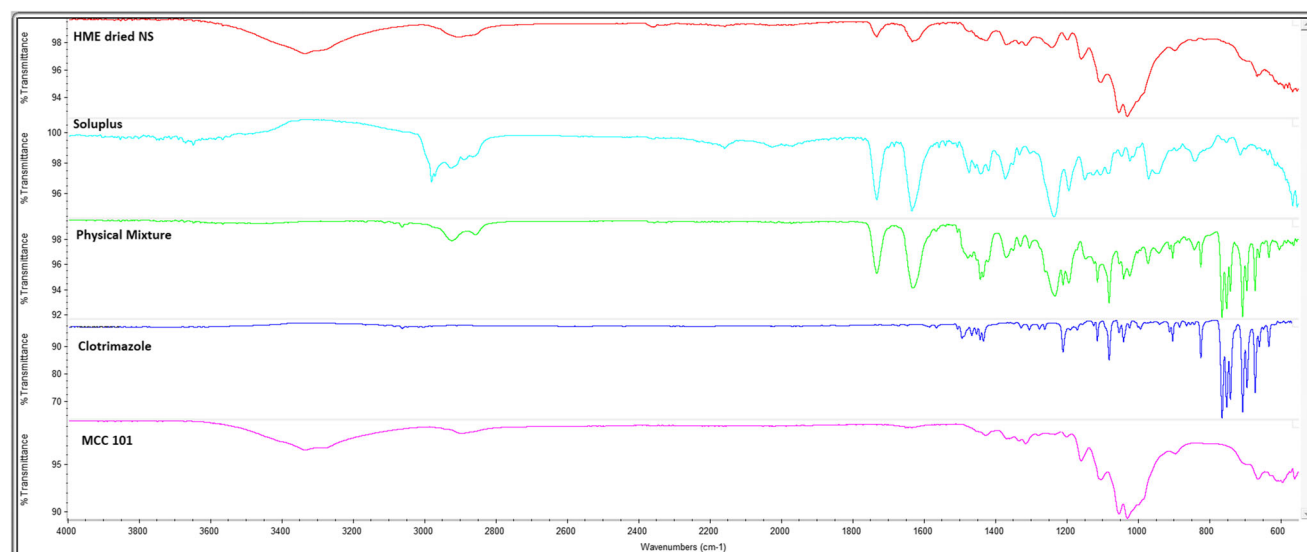


**Fig. 12.** FTIR spectra of pure clotrimazole, MCC 101, Soluplus, HME-dried nanosuspension, and physical mixture

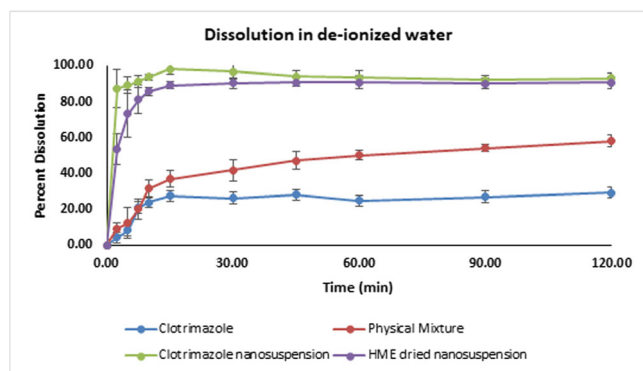


**Fig. 13.** Dissolution profiles of clotrimazole, clotrimazole nanosuspension, clotrimazole microsuspension, and clotrimazole HME-dried nanosuspension in deionized water

results of the experimental and predicted responses appear to be in close agreement, thus demonstrating the reliability of DOE approach to solidify amorphous clotrimazole nanosuspension using HME drying process.

### Polarized Light Microscopy

The pure clotrimazole and semi-crystalline MCC 101 displayed birefringence. Soluplus<sup>®</sup> which was incorporated as a polymeric stabilizer did not show any birefringence, affirming its amorphous form. The clotrimazole nanosuspension prepared by sonoprecipitation technique, devoid of MCC 101, did not exhibit any birefringence confirming the amorphous nature of clotrimazole nanoparticles. On the contrary, a physical mixture of clotrimazole suspension showed birefringence affirming the crystalline state of API. HME-dried clotrimazole nanosuspension showed extensive birefringence possibly due to the presence of excess MCC 101 which was used as a bulking agent during extrusion. Thus, PLM could not be successfully applied to evaluate the crystallinity of the drug moiety in the HME-dried end product (Fig. 9).

### Differential Scanning Calorimetry

The endothermic peak was observed at 147°C for crystalline clotrimazole, whereas amorphous Soluplus as expected did not show a melting peak. MCC 101 shows an endothermic peak at 321°C. HME-dried clotrimazole nanosuspension did not show any characteristic endothermic peak for clotrimazole confirming its amorphous nature in the drug-polymer matrix as illustrated in Fig. 10. A minor endothermic peak pertaining to clotrimazole was observed in the physical mixture. The reduction in the drug enthalpy in the physical mixture can be due to the dilution effect in the presence of excipients.

### X-ray Powder Diffraction

XRPD technique served as an orthogonal technique used to validate the DSC results. The characteristic diffraction peaks of pure crystalline clotrimazole are 9.40°, 12.61°, and 18.61°. As shown in Fig. 11, characteristic clotrimazole peaks are absent in the HME-dried end product confirming the amorphous state of clotrimazole nanoparticles. Furthermore, characteristic diffraction peaks pertaining to crystalline clotrimazole are present in the physical mixture. The characteristic crystalline peaks observed at 2θ values of 9.40°, 12.61°, and 18.61° have reduced intensities which can presumably be due to the dilution effect of API in the presence of high amount of excipient.

### Fourier Transform Infrared Spectroscopy

Infrared spectra of pure clotrimazole show peaks characteristic to C-H stretching at 3063.13 cm<sup>-1</sup> and C-Cl stretching vibration at 751.81 cm<sup>-1</sup> (45,46). The spectra of Soluplus<sup>®</sup> have transmittance peaks at 1732 cm<sup>-1</sup> and C-H stretching vibration at 2980.36 cm<sup>-1</sup>, whereas MCC 101 has characteristic O-H stretching peaks at 3280 cm<sup>-1</sup> and 3335.47 cm<sup>-1</sup> (47). Spectra of HME-dried nanosuspension and the physical mixture were similar to the addition spectra

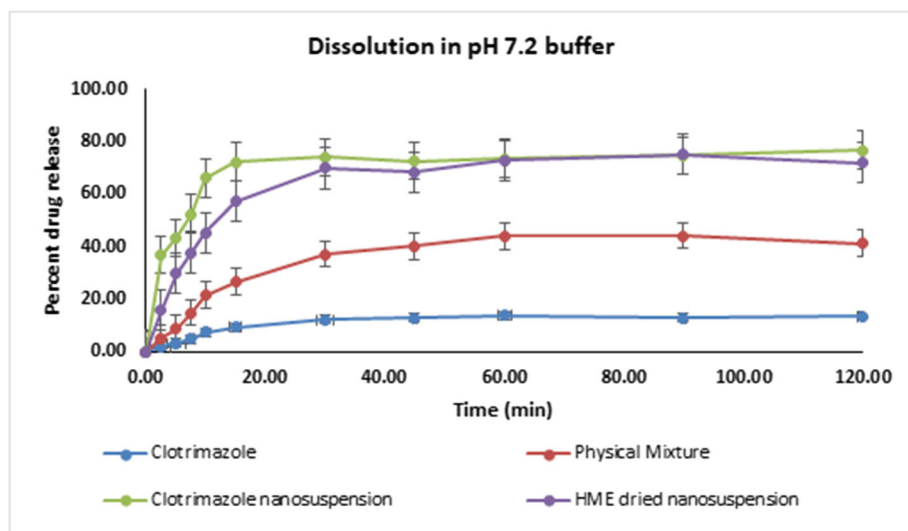


**Fig. 14.** Dissolution profiles of clotrimazole, clotrimazole nanosuspension, clotrimazole microsuspension, and clotrimazole HME-dried nanosuspension in pH 7.2 buffer

of individual components, which shows the absence of any interaction between clotrimazole and excipients (Fig. 12).

### *In Vitro* Dissolution

A higher dissolution rate was observed for clotrimazole nanosuspension and HME-dried clotrimazole nanosuspension compared to controls, neat clotrimazole, and physical mixture. Relatively higher dissolution rate was found for clotrimazole nanosuspension compared to HME-dried nanosuspension at initial time points, possibly due to the formation of loose nanoaggregates while drying in a hot melt extruder. These loose nanoaggregates may take few minutes to completely redisperse and facilitate unhindered dissolution of clotrimazole. The nanosized amorphous clotrimazole due to the virtue of high Gibb's free energy and high surface to volume ratio rapidly undergoes dissolution compared to the physical mixture and neat clotrimazole. The clotrimazole nanoamorphous suspension attained 86.74% drug release in 20 min, whereas HME-dried clotrimazole nanosuspension, micronized clotrimazole formulation, and neat clotrimazole achieved 80.34, 46.66, and 26.32% drug release respectively in deionized water (Fig. 13). Furthermore, in pH 7.2 buffer, clotrimazole nanoamorphous suspension attained 76.88% drug release in 20 min, whereas HME-dried clotrimazole nanosuspension, micronized clotrimazole formulation, and neat clotrimazole achieved 69.91, 37.23, and 12.22% drug release respectively (Fig. 14). A relatively lower drug release was observed for all the formulations in alkaline (pH 7.2 buffer) dissolution media. This lower drug release is due to the commonly observed malabsorption of weakly basic drugs under higher gastric pH conditions (48).

### CONCLUSIONS

Hot melt extruder has been successfully used as a novel technique for continuous drying of low-dose amorphous nanosuspension, resulting in embedment of drug moiety in a polymer matrix. The nanosized drug particles play a vital role in enhancing the kinetic solubility of the drug along with the enhanced solubilizing effects of the polymer matrix. An optimized drying process can help maintain the integrity of nanosized particles by preventing its agglomeration in the presence of moisture and heat energy. HME drying process parameters such as inlet temperature, screw speed, and feed rate have been explored and optimized to solidify nanosuspension by QbD approach. The optimization of HME drying process resulted in achieving higher process yield and optimum moisture content and RDI. A relatively high inlet temperature and low feed rate were critical process parameters influencing the redispersibility of drug nanoparticles after HME drying. The moderate inlet temperature increases the overall thermal energy sufficient enough to evaporate the solvent, whereas a low feed rate provides for efficient drying of nanosuspension. Thus, it can be inferred that an appropriate experimental design along with statistical analysis can result in an optimal process which delivers a drug product with desired critical quality attributes.

### REFERENCES

1. Pu X, Sun J, Li M, He Z. Formulation of nanosuspensions as a new approach for the delivery of poorly soluble drugs. *Curr Nanosci.* 2009;5(4):417–27.
2. Babu NJ, Nangia A. Solubility advantage of amorphous drugs and pharmaceutical cocrystals. *Cryst Growth Des.* 2011;11(7):2662–79.
3. Desai C, Prabhakar B. Nano-amorphous composites of cilostazol-HP- $\beta$ -CD inclusion complexes: physicochemical characterization, structure elucidation, thermodynamic studies and in vitro evaluation. *J Incl Phenom Macrocycl Chem.* 2015;81(1–2):175–91.
4. Memişoğlu E, Bochot A, Özalp M, Şen M, Duchêne D, Hincal AA. Direct formation of nanospheres from amphiphilic  $\beta$ -cyclodextrin inclusion complexes. *Pharm Res.* 2003;20(1):117–25.
5. Patel AA. Liquid salt as green solvent: a novel eco-friendly technique to enhance solubility and stability of poorly soluble drugs: Long Island University, The Brooklyn Center. 2015.
6. Vogt M, Kunath K, Dressman JB. Dissolution enhancement of fenofibrate by micronization, cogrinding and spray-drying: comparison with commercial preparations. *Eur J Pharm Biopharm.* 2008;68(2):283–8.
7. Shah DA. To understand the thermodynamic and kinetic properties of nanocrystals using poorly soluble drugs: Long Island University, The Brooklyn Center. 2015.
8. Thakuria R, Delori A, Jones W, Lipert MP, Roy L, Rodríguez-Hornedo N. Pharmaceutical cocrystals and poorly soluble drugs. *Int J Pharm.* 2013;453(1):101–25.
9. Dugar RP, Gajera BY, Dave RH. Fusion method for solubility and dissolution rate enhancement of ibuprofen using block copolymer poloxamer 407. *AAPS PharmSciTech.* 2016;17(6):1428–40.
10. Tank D, Karan K, Gajera BY, Dave RH. Investigate the effect of solvents on wet granulation of microcrystalline cellulose using hydroxypropyl methylcellulose as a binder and evaluation of rheological and thermal characteristics of granules. *Saudi Pharm J.* 2018;26(4):593–602.
11. Brough C, Williams III R. Amorphous solid dispersions and nano-crystal technologies for poorly water-soluble drug delivery. *Int J Pharm.* 2013;453(1):157–66.
12. Murdande SB, Pikal MJ, Shanker RM, Bogner RH. Solubility advantage of amorphous pharmaceuticals: I. A thermodynamic analysis. *J Pharm Sci.* 2010;99(3):1254–64.
13. Bates S, Zografi G, Engers D, Morris K, Crowley K, Newman A. Analysis of amorphous and nanocrystalline solids from their X-ray diffraction patterns. *Pharm Res.* 2006;23(10):2333–49.
14. Hancock BC, Zografi G. Characteristics and significance of the amorphous state in pharmaceutical systems. *J Pharm Sci.* 1997;86(1):1–12.
15. Laitinen R, Löbmann K, Strachan CJ, Grohgan H, Rades T. Emerging trends in the stabilization of amorphous drugs. *Int J Pharm.* 2013;453(1):65–79.
16. Laitinen R, Löbmann K, Grohgan H, Priemel P, Strachan CJ, Rades T. Supersaturating drug delivery systems: the potential of co-amorphous drug formulations. *Int J Pharm.* 2017;532:1–12.
17. Baghel S, Cathcart H, O'Reilly NJ. Polymeric amorphous solid dispersions: a review of amorphization, crystallization, stabilization, solid-state characterization, and aqueous solubilization of biopharmaceutical classification system class II drugs. *J Pharm Sci.* 2016;105(9):2527–44.
18. Chaudhari SP, Dave RH. Evaluating the effects of different molecular weights of polymers in stabilizing supersaturated drug solutions and formulations using various methodologies of the model drug: fenofibrate. *J Pharm Sci Pharmacol.* 2015;2(3):259–76.
19. Ruddy SB, Eickhoff WM, Liversidge G. Site-specific adhesion within the GI tract using nanoparticles stabilized by high molecular weight, linear poly (ethylene oxide) polymers. *Google Patents.* 1996.
20. Mittal G, Sahana D, Bhardwaj V, Kumar MR. Estradiol loaded PLGA nanoparticles for oral administration: effect of polymer molecular weight and copolymer composition on release



- behavior in vitro and in vivo. *J Control Release*. 2007;119(1):77–85.
21. Mostafa AA, Zazou MH, Chow LC, Mahmoud AA, Zaki DY, Basha M, et al. Injectable nanoamorphous calcium phosphate based in situ gel systems for the treatment of periapical lesions. *Biomed Mater*. 2015;10(6):065006.
  22. R Serrano D, H Gallagher K, Marie Healy A. Emerging nanonisation technologies: tailoring crystalline versus amorphous nanomaterials. *Curr Top Med Chem*. 2015;15(22):2327–40.
  23. Jog R, Kumar S, Shen J, Jugade N, Tan DCT, Gokhale R, et al. Formulation design and evaluation of amorphous ABT-102 nanoparticles. *Int J Pharm*. 2016;498(1):153–69.
  24. Kumar S, Shen J, Burgess DJ. Nano-amorphous spray dried powder to improve oral bioavailability of itraconazole. *J Control Release*. 2014;192:95–102.
  25. Yamasaki K, Kwok PCL, Fukushige K, Prud'homme RK, Chan H-K. Enhanced dissolution of inhalable cyclosporine nano-matrix particles with mannitol as matrix former. *Int J Pharm*. 2011;420(1):34–42.
  26. Abdelwahed W, Degobert G, Stainmesse S, Fessi H. Freeze-drying of nanoparticles: formulation, process and storage considerations. *Adv Drug Deliv Rev*. 2006;58(15):1688–713.
  27. Bohr A, Water J, Beck-Broichsitter M, Yang M. Nanoembedded microparticles for stabilization and delivery of drug-loaded nanoparticles. *Curr Pharm Des*. 2015;21(40):5829–44.
  28. Kumar S, Gokhale R, Burgess DJ. Sugars as bulking agents to prevent nano-crystal aggregation during spray or freeze-drying. *Int J Pharm*. 2014;471(1–2):303–11.
  29. Cerdeira AM, Mazzotti M, Gander B. Formulation and drying of miconazole and itraconazole nanosuspensions. *Int J Pharm*. 2013;443(1–2):209–20.
  30. Dan J, Ma Y, Yue P, Xie Y, Zheng Q, Hu P, et al. Microcrystalline cellulose-carboxymethyl cellulose sodium as an effective dispersant for drug nanocrystals: a case study. *Carbohydr Polym*. 2016;136:499–506.
  31. Sofie V, Jan V, Ludo F, Patrick A. Microcrystalline cellulose, a useful alternative for sucrose as a matrix former during freeze-drying of drug nanosuspensions—a case study with itraconazole. *Eur J Pharm Biopharm*. 2008;70(2):590–6.
  32. Maniruzzaman M, Nokhodchi A. Continuous manufacturing via hot-melt extrusion and scale up: regulatory matters. *Drug Discov Today*. 2017;22(2):340–51.
  33. Baumgartner R, Eitzlmayr A, Matsko N, Tetyczka C, Khinast J, Roblegg E. Nano-extrusion: a promising tool for continuous manufacturing of solid nano-formulations. *Int J Pharm*. 2014;477(1):1–11.
  34. Hao J, Fang X, Zhou Y, Wang J, Guo F, Li F, et al. Development and optimization of solid lipid nanoparticle formulation for ophthalmic delivery of chloramphenicol using a Box-Behnken design. *Int J Nanomedicine*. 2011;6:683.
  35. Sharma D, Maheshwari D, Philip G, Rana R, Bhatia S, Singh M, et al. Formulation and optimization of polymeric nanoparticles for intranasal delivery of lorazepam using Box-Behnken design: in vitro and in vivo evaluation. *Biomed Res Int*. 2014;2014:1–14.
  36. Nekkanti V, Muniyappan T, Karatgi P, Hari MS, Marella S, Pillai R. Spray-drying process optimization for manufacture of drug-cyclodextrin complex powder using design of experiments. *Drug Dev Ind Pharm*. 2009;35(10):1219–29.
  37. Mishra B, Sahoo J, Dixit PK. Enhanced bioavailability of cinnarizine nanosuspensions by particle size engineering: optimization and physicochemical investigations. *Mater Sci Eng C*. 2016;63:62–9.
  38. Thakkar HP, Patel BV, Thakkar SP. Development and characterization of nanosuspensions of olmesartan medoxomil for bioavailability enhancement. *J Pharm Bioallied Sci*. 2011;3(3):426–34.
  39. Zhang X, Liu J, Qiao H, Liu H, Ni J, Zhang W, et al. Formulation optimization of dihydroartemisinin nanostructured lipid carrier using response surface methodology. *Powder Technol*. 2010;197(1–2):120–8.
  40. Talekari SD, Dave RH. Solubility enhancement of a BCS class II drug using granulated fumed silica as an adsorbent. *J Pharm Res* 2017;18(6):1–15. <https://doi.org/10.9734/JPR1/2017/36872>.
  41. Gajera BY, Dugar RP, Dave RH. Formulation development and optimization of ibuprofen poloxamer melt granules using hydrophilic excipients. *Br J Pharm Res*. 2016;13(6):1–19.
  42. Lu Y, Yu Y, Tang X. Sucrose acetate isobutyrate as an in situ forming system for sustained risperidone release. *J Pharm Sci*. 2007;96(12):3252–62.
  43. Crowley MM, Zhang F, Repka MA, Thumma S, Upadhye SB, Kumar Battu S, et al. Pharmaceutical applications of hot-melt extrusion: part I. *Drug Dev Ind Pharm*. 2007;33(9):909–26.
  44. Quek SY, Chok NK, Swedlund P. The physicochemical properties of spray-dried watermelon powders. *Chem Eng Process Process Intensif*. 2007;46(5):386–92.
  45. Madgulkar A, Bandivadekar M, Shid T, Rao S. Sugars as solid dispersion carrier to improve solubility and dissolution of the BCS class II drug: clotrimazole. *Drug Dev Ind Pharm*. 2016;42(1):28–38.
  46. Karolewicz B, Gajda M, Owczarek A, Pluta J, Górniak A. Physicochemical characterization and dissolution studies of solid dispersions of clotrimazole with Pluronic F127. *Trop J Pharm Res*. 2014;13(8):1225–32.
  47. Pachua L, Vanlalfakawma DC, Tripathi SK, Lalhlenmawia H. Muli bamboo (*Melocanna baccifera*) as a new source of microcrystalline cellulose. 2014.
  48. Mitra A, Kesisoglou F. Impaired drug absorption due to high stomach pH: a review of strategies for mitigation of such effect to enable pharmaceutical product development. *Mol Pharm*. 2013;10(11):3970–9.